In addition to the red needles described we obtained small orange plates of another modification of **1** under different reaction conditions. Furthermore, the red phase slowly changes into a yellow one at low temperature. Thus investigations on the phase relations as well as efforts to solve the formation mechanism of **1** are in progress.

Experimental Section

catena-Poly{[tetrakis(μ-trifluoroacetato-$\kappa O,\kappa O'$)dibismuth($Bi-Bi$)]-μ-η^6-hexamethylbenzene} (**1**): A mixture of $Bi(O_2CCF_3)_3$[3b] (0.010 g, 0.18 mmol) and freshly sublimed hexamethylbenzene (0.020 g, 0.12 mmol) in a sealed Duran glass tube was heated to 100 °C in an aluminum block oven. Small light yellow plates of $Bi(O_2CCF_3)_3 \cdot 0.5\,C_{12}H_{18}$ which initially grew at the glass surface disappeared in the course of several weeks, while dark red needles of **1** grew (0.019 g, 20.5 % isolated; a yellow-gray residue remained). Elemental analysis calcd for ($M_r = 1032.30$) (%): C 23.1, H 1.7; found: C 22.1, H 1.8; MS (EI, 70 eV, 1.0 mA, QT = 220 °C): *m/z* (%): 870 (9) [$(\mathbf{1}-C_{12}H_{18})^+$], 757 (24) [$(Bi_2(O_2CCF_3)_3)^+$], 644(7) [$(Bi_2(O_2CCF_3)_2)^+$], 531(6) [$(Bi_2(O_2CCF_3))^+$], 435 (8) [$(Bi(O_2CCF_3)_2)^+$], 418 (6) [$Bi_2^+$], 322(19) [$(Bi(O_2CCF_3))^+$], 209 (50) [$Bi^+$], 162 (57) [$C_{12}H_{18}^+$], 147 (100) [$C_{11}H_{15}^+$].

Received: June 22, 1998 [Z 12017 IE]
German version: *Angew. Chem.* **1998**, *110*, 3153 – 3155

Keywords: arene complexes · bismuth · carboxylato complexes · metal – metal interactions · stacking interactions

[1] a) F. A. Cotton, R. A. Walton, *Multiple Bonds Between Metal Atoms*, 2nd ed., Oxford University Press, Oxford, **1992**; b) F. A. Cotton, R. A. Walton, *Struct. Bonding* **1985**, *62*, 1; c) F. A. Cotton, M. H. Chisholm, *Chem. Eng. News* **1982**, *60*, 40; d) F. A. Cotton, *Chem. Soc. Rev.* **1983**, *12*, 35; e) M. H. Chisholm, I. P. Rothwell, *Progr. Inorg. Chem.* **1982**, *29*, 1.

[2] a) H. Binder, B. Brellochs, B. Frei, A. Simon, B. Hettich, C*hem. Ber.* **1989**, *122*, 1049; b) W. Uhl, I. Hahn, H. Reuter, *ibid.* **1996**, *129*, 1425; c) S. Adams, M. Dräger, B. Mathiasch, *J. Organomet. Chem.* **1987**, *326*, 186.

[3] a) P. V. Radheshwar, R. Dev, G. H. Cady, *J. Inorg. Nucl. Chem.* **1972**, *34*, 3913. b) G. J. Reiß, W. Frank, J. Schneider, *Main Group Metal Chem.* **1995**, *18*, 287.

[4] $C_{20}H_{18}Bi_2F_{12}O_8$, $M_r = 1032.30$; crystal dimensions: $0.02 \times 0.02 \times 0.1$ mm^3, monoclinic, space group $C2/m$, $a = 19.963(4)$, $b = 9.053(2)$, $c = 9.040(2)$ Å, $\beta = 109.22(3)^\circ$, $Z = 2$, $V = 1542.7(6)$ Å^3, $\rho_{calcd} = 2.222$ Mg m^{-3}, $T = -10 \pm 1$ °C, $2\theta_{max} = 52.1^\circ$, STOE-IPDS, $Mo_{K\alpha}$ radiation ($\lambda = 0.71073$ Å), 5558 measured, 1397 unique, and 1321 observed reflections with $I > 2\sigma(I)$, LP correction ($\mu = 11.50$ mm^{-1}), Patterson method and ΔF synthesis, minimization of $\Sigma w(F_o^2 - F_c^2)^2$ with $w = 1/[\sigma^2(F_o^2) + (0.0599\,P)^2]$ where $P = (F_o^2 + 2F_c^2)/3$, 114 refined paramters, $R_1 = 0.0367$, $wR_2 = 0.0850$; $\Delta\rho_{max}/\Delta\rho_{min} + 1.18/-1.37$ e Å^{-3}. Crystallographic data (excluding structure factors) for the structure reported in this paper have been deposited with the Cambridge Crystallographic Data Center as supplementary publication no. CCDC-102011. Copies of the data can be obtained free of charge on application to CCDC, 12 Union Road, Cambridge CB2 1EZ, UK (fax: (+44) 1223-336-033; e-mail: deposit@ccdc.cam.ac.uk).

[5] The figures in this paper were drawn on basis of ORTEX images (P. McArdle, *J. Appl. Cryst.* **1995**, *28*, 65) with RASTEP and RENDER (E. A. Merrit, D. J. Bacon, *Meth. Enzymol.* **1997**, *277*, 505).

[6] a) A. Schier, J. M. Wallis, G. Müller, H. Schmidbaur, *Angew. Chem.* **1986**, *98*, 742; *Angew. Chem. Int. Ed. Engl.* **1986**, *25*, 757; b) W. Frank, J. Weber, E. Fuchs, *Angew. Chem.* **1987**, *99*, 68; *Angew. Chem. Int. Ed. Engl.* **1987**, *26*, 74.

[7] a) O. Mundt, G. Becker, M. Rössler, C. Witthauer, *Z. Anorg. Allg. Chem.* **1983**, *506*, 42; b) A. J. Ashe, III, J. W. Kampf, D. B. Puranik, A. M. Al-Taweel, *Organometallics* **1992**, *11*, 2743; c) F. Calderazzo, A. Morvillo, G. Pelizzi, R. Poli, *J. Chem. Soc. Chem. Commun.* **1983**, 507; d) F. Calderazzo, R. Poli, G. Pelizzi, *J. Chem. Soc. Dalton Trans.* **1984**, 2365; e) K. H. Whitmire, J. M. Cassidy, *Acta Crystallogr. Sect. C* **1992**, *48*, 917.

[8] N. Tokitoh, Y. Arai, R. Okazaki, *Science* **1997**, *277*, 78.

[9] W. Frank, G. J. Reiß, J. Schneider, *Angew. Chem.* **1995**, *107*, 2572; *Angew. Chem. Int. Ed. Engl.* **1995**, *34*, 2416.

Cooperative Hydrogen Bonding and Enzyme Catalysis**

Hong Guo* and Dennis R. Salahub*

Understanding the structural basis for stabilization of transition states in enzyme-catalyzed reactions is of fundamental importance. Such knowledge would help to improve existing enzymes and to design new ones.[1, 2] High-resolution structures have revealed important features at enzyme active sites.[3, 4] However, identification of the key factors responsible for the catalysis has proven to be difficult[5, 6] owing to the complexity of interactions that obscure the underlying mechanisms. This is the case for stabilization of transition states involving α helices, for example. Although the ability of the helices to stabilize negatively charged reaction intermediates and transition states has been well established,[2, 3, 7] the origin of the charge stabilization is still uncertain.[3, 5]

Here we report results of density functional calculations which reveal a large cooperative effect induced by the interaction of an anion with a peptide hydrogen bond network, directly or through an imidazole (Im) molecule. The major contribution to this cooperativity consists of nonadditive, many-body effects that can not be reflected by the pair-wise interactions of the charged ligand with the individual peptide units involved, and that are closely associated with the presence of the hydrogen-bond network. The increase of the cooperative effect on going from a neutral to a negatively charged ligand is sufficiently large that it could make an important contribution to the catalysis by stabilizing the charge formation along the reaction pathway in the enzyme-catalyzed reactions. The mechanism proposed here, based on the enhancement of cooperative hydrogen bonding, provides a consistent interpretation for both the wide occurrence of helices at enzyme active sites[3] and phosphate (sulfate) binding sites[7] as well as their absence in some instances.[8–11]

[*] Dr. H. Guo, Prof. D. R. Salahub
Centre de Recherche en Calcul Appliqué
5160, boul. Décarie, bureau 400
Montréal, Québec, H3X 2H9 (Canada)
and
Département de chimie, Université de Montréal
C.P. 6128 Succursale centre-ville
Montréal, Québec, H3C 3J7 (Canada)
Fax: (+1) 514-343-2468
E-mail: dennis.salahub@umontreal.ca

[**] Support for parts of this work from Biosym Technologies and from Astra Research Centre, Montreal, is gratefully acknowledged.

Although the existence of a cooperative effect in peptide and imidazole hydrogen bonding is known[12] and differential cooperativities have been proposed for the interpretation of other phenomena,[12b] such large π cooperativity and many-body effects have not been detected and their role in enzyme catalysis has not been discussed previously. The results of quantum mechanical calculations also suggest that helices with an α_N-type distortion[13] at the N terminus may be even more effective in the charge stabilization. The relationship between the cooperative hydrogen bonding and low-barrier hydrogen bonds[4] in enzyme catalysis is also discussed.

The model systems for peptide hydrogen bond networks used in this study are given in Figure 1 a. They include

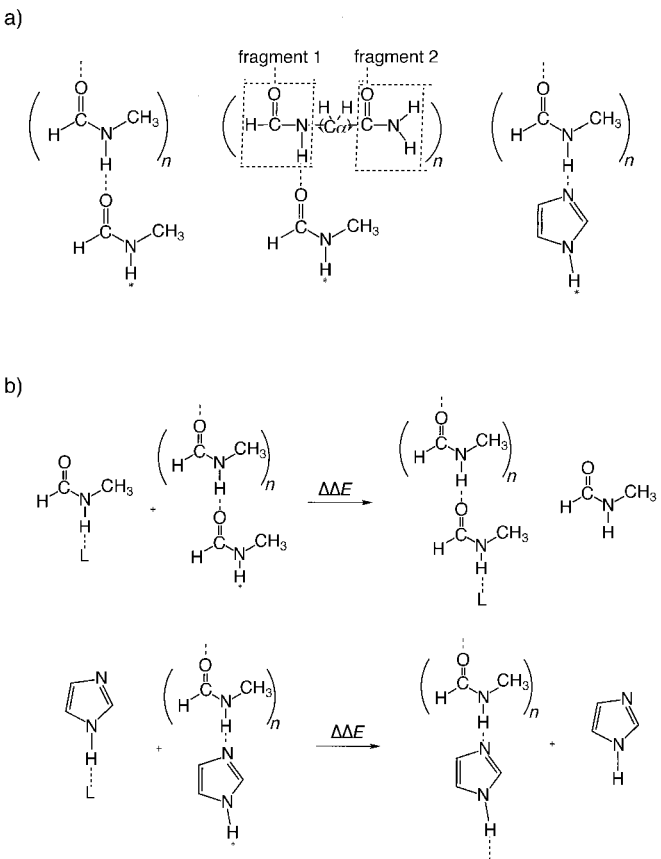

Figure 1. a) Model systems for peptide hydrogen bond networks used in this study. The star designates the binding site. From left to right: NMF$\cdots$(NMF)$_n$, NMF$\cdots$(GDA)$_n$, and Im$\cdots$(NMF)$_n$. (GDA)$_n$ contains two hydrogen-bonded peptide fragments, fragments 1 and 2, that are separated by the C_α carbon atoms. The initial structures of NMF$\cdots$(GDA)$_n$ for geometry optimizations were build from GDAs with $(\varphi,\psi)=(-60,-50^\circ)$. The final φ and ψ angles for NMF$\cdots$(GDA)$_n$ are (starting from the GDA next to NMF): for $n=2$, $(\varphi_1,\psi_1)=(-83,-20^\circ)$ and $(\varphi_2,\psi_2)=(-120,14^\circ)$; for $n=3$, $(\varphi_1,\psi_1)=(-80,-24^\circ)$, $(\varphi_2,\psi_2)=(-80,-24^\circ)$, and $(\varphi_3,\psi_3)=(-115,10^\circ)$. The φ and ψ angles for NMF$\cdots$(GDA$\cdot$2H$_2$O)$\cdots$GDA (see text) are: $(\varphi_1,\psi_1)=(-86,-16^\circ)$ and $(\varphi_2,\psi_2)=(-117,15^\circ)$. The geometry optimizations of NMF$\cdots$(GDA)$_n$ lead to stable conformations in which the carbonyl group of NMF forms only one hydrogen bond to the terminal NH group of fragment 1 of (GDA)$_n$. b) The processes used to determine the cooperative effects ($\Delta\Delta E_n$). Different definitions for the cooperativity have been used in the literature. The cooperative effect defined here also includes the two-body interactions of nonneighbors in addition to the many-body terms. Top: NMF$\cdots$(NMF)$_n$ is involved. Bottom: Im$\cdots$(NMF)$_n$ is involved. The process involving NMF$\cdots$(GDA)$_n$, NMF$\cdots$2(H$_2$O)$_6$, and NMF$\cdots$2(H$_2$O)$_8$ (not shown) are similar.

hydrogen-bonded *N*-methylformamide oligomers (NMF$\cdots$(NMF)$_n$, $n=1-4$) and NMF/GDA complexes (NMF$\cdots$(GDA)$_n$, $n=2$, 3), where GDA stands for a glycine dipeptide analogue.[14] We also use Im$\cdots$(NMF)$_n$ complexes for which the "N-terminal" NMF in NMF$\cdots$(NMF)$_n$ is replaced by imidazole.

We consider the exchange processes illustrated in Figure 1 b, where a neutral or anionic ligand (L) moves from the NMF or Im binding site to the binding site in the corresponding system with peptide hydrogen bond network(s). The energy changes for the processes are referred to as the cooperative effects ($\Delta\Delta E_n$)[15] that are induced by the ligand binding to the systems with the hydrogen-bonding network. The effectiveness of the peptide hydrogen bond networks in inducing cooperative effects is compared with those induced by two stable water hexamers or octamers (NMF$\cdots$2(H$_2$O)$_6$ and NMF$\cdot$2(H$_2$O)$_8$; see Figure 2 c).

The ball-and-stick representations for some of the systems are plotted in Figure 2. Different procedures may be used for the evaluation of the cooperative effects. The structures of all the systems involved in the process may be optimized, and the energies at these optimized geometries can then be used to determine the $\Delta\Delta E$ value. Alternatively, one can apply certain structural constraints to some of the systems. Two types of structural constraints have been considered in this work, in addition to the full geometry optimizations. In type A, the constraints are used only for the systems *with* a ligand (e.g., L$\cdots$NMF and L$\cdots$NMF$\cdots$(GDA)$_n$). Here geometry optimization was performed for the ligand and the N–H bond interacting with the ligand, whereas the rest of the structural parameters were fixed at the values found in the corresponding systems without the ligand (e.g., NMF and NMF$\cdots$(GDA)$_n$). In type B, the constraints are applied to the systems *without* a ligand (e.g., NMF and NMF$\cdots$(GDA)$_n$), for which only single-point calculations were performed at the structures found in the corresponding systems with a ligand (e.g., L$\cdots$NMF and L$\cdots$NMF$\cdots$(GDA)$_n$).

The $\Delta\Delta E_n$ values are listed in Table 1. The methods of density functional theory[16] have been used in this study with generalized gradient approximation functionals of the Becke–Perdew (BP) type. Three levels of calculation (BP/DZVP, BP/6-311++G** and BP/6-311++G**//BP/DZVP) have been performed, but only the BP/DZVP values are given here since the $\Delta\Delta E_n$ values are not very sensitive to the basis set and no new information was obtained. As is evident from Table 1, for neutral ligands $\Delta\Delta E_n$ is only about -1 to -2 kcal mol^{-1}, consistent with previous theoretical and experimental results.[12] In contrast, the cooperative effects are much larger (-7 to -35 kcal mol^{-1}) for the cases involving negatively charged groups, and they are not very sensitive to the nature of the anions involved. Thus, there is a large increase of $\Delta\Delta E_n$ in going from neutral to anionic ligands. Introducing solvent molecules on HCO_2^- reduces $\Delta\Delta E$ by only about 2–4 kcal mol^{-1}. The value of $\Delta\Delta E_n$ increases with increasing size of the system (n), and the replacement of the NMF interacting with the anions by Im leads to similar results; a large cooperative effect was also observed when the NMF molecule was replaced by CH_3OH. We will call such hydrogen-bonding networks with the Im and/or hydroxyl extension

  1433-7851/98/3721-2986 $ 17.50+.50/0

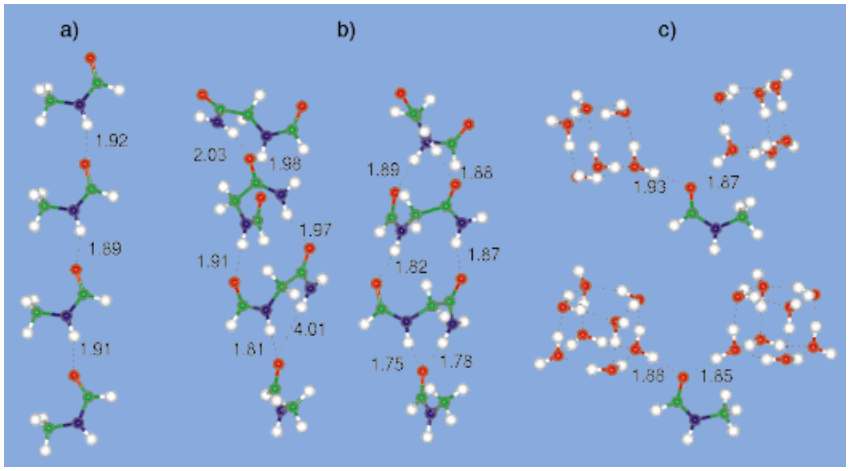

Figure 2. Ball-and-stick representations for some of the systems. Hydrogen bonds are designated by dashed lines. a) $NMF\cdots(NMF)_3$; b) $NMF\cdots(GDA)_3$; left: fully optimized structure; right: the structure with constraints of type B. c) $NMF\cdots2(H_2O)_{2n}$; top: $NMF\cdots2(H_2O)_6$; bottom: $NMF\cdots2(H_2O)_8$.

Table 1. Cooperative effects [kcal mol^{-1}] induced by the interactions of ligands with hydrogen-bond networks.[a]

Hydrogen-bond network	Ligand (L)	$\Delta\Delta E_n$			
		$n=1$	$n=2$	$n=3$	$n=4$
$NMF\cdots(NMF)_n$	H_2O	−1.1	−1.7	−1.8	−1.9
	HCO_2H	−1.3			
	Im	−1.8			
	HCO_2^-	−9.9	−13.8	−15.9	−17.2
	Im^-	−9.2			
	CH_3S^-	−9.0			
	$H_2PO_4^-$	−8.2			
	$2H_2O\cdots HCO_2^-$	−7.6	−10.7	−12.4	
	$H_2O\cdots H_2O\cdots HCO_2^-$	−6.8		−12.1	
$NMF\cdots(NMF)_n$[b]	HCO_2^-	−8.6	−12.7	−14.4	
$NMF\cdots(NMF)_n$[c]	HCO_2^-	−11.7	−16.9	−19.1	
$NMF\cdots(GDA)_n$	HCO_2^-		−22.4	−26.4	
$NMF\cdots(GDA)_n$[b]	HCO_2^-		−16.4	−20.3	
$NMF\cdots(GDA)_n$[c]	HCO_2^-		−29.2	−35.1	
$NMF\cdots(GDA\,2H_2O)\cdots GDA$[b]	HCO_2^-		−16.4		
$Im\cdots(NMF)_n$	H_2O	−1.1	−1.6		
	HCO_2^-	−10.1	−15.0		
	$2H_2O\cdots HCO_2^-$	−7.7	−11.7		
$NMF\cdots2(H_2O)_{2n}$	HCO_2^-			−16.3	−15.1

[a] BP/DZVP values. Except where otherwise noted, full geometry optimizations have been performed. For most of the cases involving formate, one of the orbitals *anti* to the C–H bond interacts with NMF or Im; the only exception is the case involving $H_2O\cdots H_2O\cdots HCO_2^-$, where one of the orbitals eclipsing the C–H bond is used. For $2H_2O\cdots HCO_2^-$, two water molecules interact, respectively, with the two orbitals of formate eclipsing the C–H bond. For $H_2O\cdots H_2O\cdots HCO_2^-$, one water donates two hydrogen bonds to the two orbitals *anti* to the C–H bond and another water donates one hydrogen bond to one of the orbitals eclipsing the C–H bond. [b] Constraints of type A applied (see text). [c] Constraints of type B applied.

augmented peptide hydrogen bond networks. Introducing two water molecules to the two carbonyl groups of the first GDA ($NMF\cdots(GDA\cdot2(H_2O)\cdots GDA$) has little effect on $\Delta\Delta E$.

The $\Delta\Delta E_n$ values obtained with the constraints of type B are greater than those obtained with the constraints of type A or with full geometry optimizations, as the systems of hydrogen-bonding networks are better adapted for the anion. This is especially true for the processes involving $NMF\cdots(GDA)_n$, where the cooperative effects obtained with the type B constraints are considerably larger, by as much as 7–15 kcal mol^{-1} (only 2–5 kcal mol^{-1} for the cases involving $NMF\cdots(NMF)_n$).

As can be seen from Figure 2b, the major structural difference for $NMF\cdots(GDA)_n$ is that with the constraints of type B the NMF molecule interacts with both NH groups from the next GDA, while it forms only one hydrogen bond to the NH group from fragment 1 in the optimized structure. Thus, the presence of HCO_2^- and the geometry optimization drive the NMF molecule to interact with the second NH group from fragment 2. To anticipate the formation of the second hydrogen bond with NMF, $(GDA)_n$ undergoes significant structural changes. Such structural changes are energetically unfavorable, as the energies of $NMF\cdots(GDA)_n$ become higher even with the compensation from the formation of the second hydrogen bond to fragment 2. Thus, the larger $\Delta\Delta E$ values are due to geometric relaxation which allows the formation of two peptide hydrogen bond networks connected to NMF, both of them being able to induce the cooperative effect. The implication of this finding to helix-charge interactions will be discussed later. As can be seen from Table 1, the two peptide hydrogen bond networks of $(GDA)_n$ are far more effective in inducing the cooperative effects than the two water clusters; the $\Delta\Delta E$ values are 6–10 kcal mol^{-1} larger than those obtained with two $(H_2O)_6$ or $(H_2O)_8$.

The energies of the pair interaction of HCO_2^- with its nonneighboring GDA or peptide units in some complexes are listed in Table 2; the fragment contributions are also given for the processes involving $NMF\cdots(GDA)_2$ using constraints of type A, that is, without anion-induced structural relaxation. The $\Delta\Delta E$ values of the fragments are additive in that the cooperative effect obtained with $(GDA)_2$ is basically the same as the sum of those from its two fragments. Fragment 1 of $(GDA)_2$ makes a major contribution (−12 kcal mol^{-1}) to the total $\Delta\Delta E$ value (−16.4 kcal mol^{-1}), while the contribution from fragment 2 is considerably smaller (−4.5 kcal mol^{-1}). Table 2 shows that the sums of the energies for pair interactions between nonneighbors are much smaller than the corresponding $\Delta\Delta E$ values in almost all cases; the only exception involves $NMF\cdots[(GDA)_2]^{frag2}$ (i.e., without a peptide hydrogen bond network connected to the anion). These analyses suggest that the many-body, nonadditive effects make a major contribution to the observed strong cooperativity and that the existence of peptide hydrogen bond networks is very important for a large energetic effect.

  1433-7851/98/3721-2987 $ 17.50+.50/0

Table 2. Energies of pair interactions between HCO_2^- and its nonneighboring units as well as the fragment contributions of $(GDA)_2$ [kcal mol^{-1}].[a]

System	1,3	1,4	1,5	Total	$\Delta\Delta E_n$
$HCO_2^- \cdots NMF \cdots (GDA)_2$[b]	−7.6	−2.6		−10.2	−22.4
$HCO_2^- \cdots NMF \cdots (GDA)_2$	−5.5	−2.1		−7.6	−16.4
$HCO_2^- \cdots NMF \cdots [GDA)_2]^{frag1}$	−3.7	−1.3		−5.0	−12.0
$HCO_2^- \cdots NMF \cdots [GDA)_2]^{frag2}$	−2.0	−1.0		−3.0	−4.5
$HCO_2^- \cdots NMF \cdots (NMF)_2$	−3.9	−1.5		−5.4	−12.7
$HCO_2^- \cdots NMF \cdots (NMF)_3$[b]	−4.2	−1.6	−0.8	−6.6	−15.9
$HCO_2^- \cdots NMF \cdots (NMF)_3$	−3.9	−1.5	−0.8	−6.2	−14.4
$H_2O \cdots H_2O \cdots HCO_2^- NMF \cdots (NMF)_3$[b]	−2.1	−1.4	−0.7	−4.2	−12.1

[a] Except where otherwise noted, constraints of type A have been applied. $[(GDA)_2]^{frag1}$ designates that fragment 2 of the system is removed from $NMF \cdots (GDA)_2$ (Figure 1a) with the $C_\alpha H_2$ groups replaced by hydrogen atoms. The positions of the hydrogen atoms were optimized based on energy minimizations, whereas the rest of the structural parameters were fixed. Standard energy decomposition techniques were used for estimating the through-space pair interactions of the anion with its nonneighboring GDAs and peptide units. In this approach, the energies of the ligand (L) and each of its nonneighboring units are determined at their relaxed structures found in $HCO_2^- \cdots NMF \cdots (NMF)_n$, $HCO_2^- \cdots NMF \cdots (GDA)_2$, or $HCO_2^- \cdots NMF \cdots [(GDA)_2]^{frag1/frag2}$, and these energies are used as the reference energies for the interactions. The interaction energies are obtained for each pair of L and its nonneighboring unit fixed at their positions according to the geometries found in the complexes. [b] Full geometry optimization was performed for this complex. $H_2O \cdots H_2O \cdots HCO_2^-$ is considered as a single unit.

The results reported here suggest that peptide or augmented peptide hydrogen bond networks could make an important contribution to the charge stabilization through cooperative interactions. The large $\Delta\Delta E$ values will undoubtedly be moderated in the real environment of the protein and will depend on the mechanism of enzyme-catalyzed reactions so that the exact contribution of the hydrogen-bonding networks to the catalysis would have to be modified accordingly. Nevertheless, the identification of strong interactions between anions and hydrogen-bonded networks as an important factor for enzyme structure and function allows us to offer detailed insight into a number of structural features observed in the neighborhood of active sites that are prepared, during the folding process, for interactions with charged ligands or intermediates. In the following we will summarize several experimental results that can be attributed to such strong cooperativity.

As a major component of protein secondary structure, α helices provide a convenient way for arranging the peptide hydrogen bond networks. The mechanism proposed here can account for the observation that isolated peptide hydrogen bond networks occur at enzyme active sites as well as at phosphate (sulfate) binding sites even though no helix is present. Serine proteases represent a well-known case which suggests that the presence of a helix may not be a necessary condition for the charge stabilization. For subtilisin, there is an active-site helix, and, consistent with an earlier interpretation based on the helix macrodipole,[3] the catalytic serine residue (S221) is located at the N terminus of the helix with its amide group involved in the oxyanion hole interactions (Figure 3a).[17]

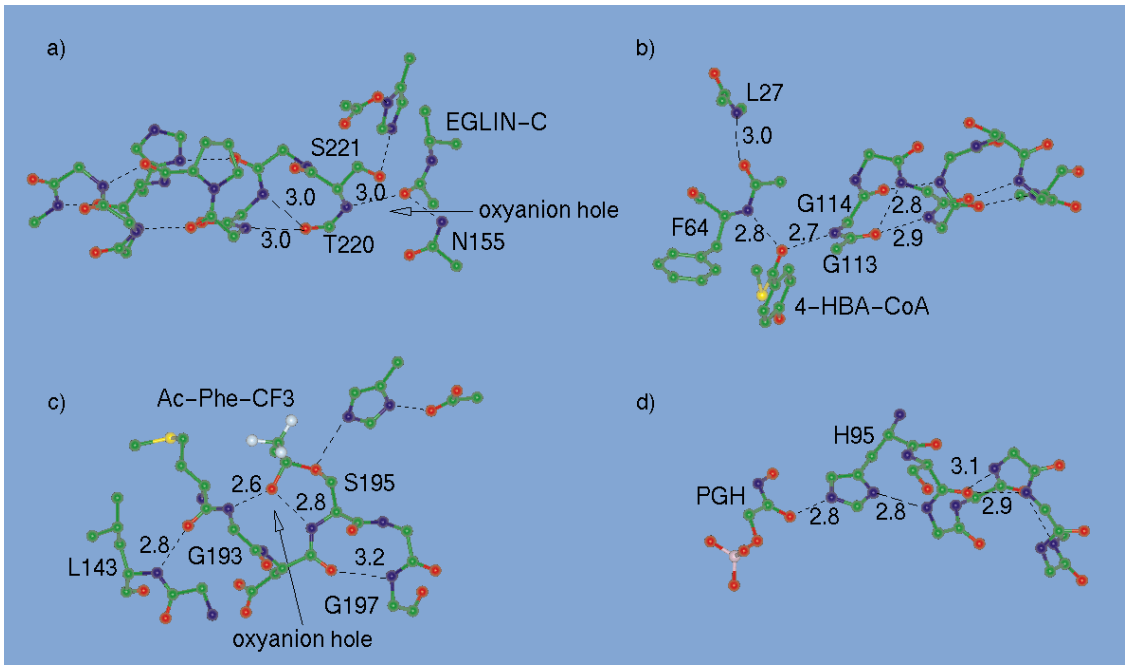

Figure 3. Examples of peptide hydrogen bond networks at enzyme active sites. Hydrogen bonds are designated by dashed lines. a) Subtilisin Carlsberg complexed with EGLIN-C.[17] The main-chain NH group of S221 interacts with EGLIN-C, and the carbonyl group of T220 is involved in a bifurcated 1–4 and 1–5 hydrogen bond in the active-site helix. b) 4-Hydroxybenzoyl-CoA (4-HBA-CoA) bound to 4-chlorobenzoyl-CoA dehalogenase.[8] An isolated peptide hydrogen bond network and an active-site helix are involved in the stabilization of the transition state. The main-chain NH group of G114 interacts with 4-HBA-CoA, and the carbonyl group of G113 is involved in a bifurcated 1–4 and 1–5 hydrogen bond in the helix. The isolated peptide hydrogen bond network involves the peptide linkage between G63 and F64 and that between A26 and L27; c) γ-Chymotrypsin complexed with Ac-Phe-CF_3.[9] Two isolated peptide hydrogen networks are involved in the stabilization of the transition state. One involves the peptide linkages between M192 and G193 and between G142 and L143, and the other involves the peptide linkages between D194 and S195 and between G196 and G197. d) Triosephosphate isomerase (TIM) complexed with phosphoglycolohydroxamate (PGH).[19] The main-chain NH group of E97 donates a hydrogen bond to H95, and the carbonyl group of S96 is involved in bifurcated 1–4 and 1–5 hydrogen bonds in an active-site helix.

  1433-7851/98/3721-2988 $ 17.50+.50/0

Such an active-site helix, however, is not present in the chymotrypsin-related serine proteases. This difference can be understood by considering cooperative effects involving peptide hydrogen bond networks. Figure 3c shows the active site of a tetrahedral transition-state complex of chymotrypsin with a peptidyl trifluoromethyl ketone (Ac-Phe-CF_3).[9] Two peptide hydrogen bond networks are connected to the negatively charged oxygen atom of Ac-Phe-CF_3 and are involved in the oxyanion hole interactions. An isolated peptide hydrogen bond network also exists at the active site of the 4-chlorobenzoyl-CoA dehalogenase/4-HBA-CoA complex,[8] where the NH group of F64 interacts with the benzoyl moiety of 4-HBA-CoA; the carbonyl group within the same peptide linkage forms a hydrogen bond to the main-chain NH group of L27 (Figure 3b). This hydrogen-bond network as well as the one involving L143 in the chymotrypsin complex do not belong to an individual helix, turn, or sheet. A previous statistical survey[13] shows that this type of backbone hydrogen bond represents only 5% of the hydrogen bonds between main chains in proteins. Thus, the occurrence of these peptide hydrogen bond networks at the enzyme active sites might be considered as rather uncommon. These structural data support the results from the quantum mechanical calculations that suggest an important role of cooperative hydrogen-bond networks (as opposed to the helix macrodipole per se) in the charge stabilization. Isolated peptide hydrogen bond networks have also been observed to interact with phosphate (sulfate) moieties in phosphate-binding (sulfate-binding) proteins,[10, 11, 18] and a possible role of the hydrogen-bonding networks in the charge stabilization has been suggested.[11]

Triosephosphate isomerase (TIM)[2, 19] represents an interesting example where a "relay" of charge might be assisted by the cooperative effect. It uses a neutral histidine residue (H95) rather than the much more electrophilic imidazolium ring to interact with the carbonyl oxygen atom of the substrate; H95 is located at the N terminus of a short α helix (Figure 3d). As mentioned earlier, a neutral imidazole can participate in cooperative hydrogen bonding and thus serves as a simple extension of the peptide hydrogen-bond network(s) from the helix. This extension could enhance the cooperative effect, as suggested from the results on the model systems. Moreover, if a proton or a partial proton transfer from the histidine residue to the reaction intermediate or substrate is involved,[2, 4, 19] the charge formation on H95 could in turn be stabilized by a stronger cooperative effect induced by the interaction of H95 with the helix. A similar discussion can be made for citrate synthase (CS), where H274 located at the N terminus of an α helix plays a similar role. Such a strategy might also be used by other enzymes in which cooperative hydrogen-bond networks are well positioned to stabilize the charge formation along the reaction pathways through an enhancement of cooperative hydrogen bonding.

As discussed earlier, a larger cooperative effect can be induced if the carbonyl group of the peptide linkage interacting with an anion (NMF in our model systems) is involved in a bifurcated hydrogen bond with the amide groups of two peptide units or hydrogen-bonded networks. There is a frequent occurrence of α_N-type distortion at the N terminus of α helices[13a] in which the carbonyl oxygen atom of residue 1 is directed between the NH groups of residues 4 and 5 and therefore involved in a bifurcated 1-4 and 1-5 hydrogen bond. A survey[13a] of the crystal structures for twelve proteins shows that there are 16 examples of the α_N distortion among 50 α helices. Based on the mechanism of cooperative hydrogen bonding, it seems that the helices with the α_N distortion might be more effective in the charge stabilization, since two of the peptide hydrogen bond networks can be used to induce the cooperative effect. Such distortion exists widely in the active-site helices. This can be seen from Figure 3, where the α_N distortion exists in all three active-site helices. The suggestion proposed here also seems to be consistent with the appearance of phosphate groups at the end of 3_{10} helices even without well-aligned peptide dipoles.[7a]

It was recently proposed that low-barrier hydrogen bonds play an important role in enzyme catalysis,[4] but the energetic effects due to the formation of low-barrier hydrogen bonds have not been well established.[6] For many of the cases where a low-barrier hydrogen bond was suggested, there are actually cooperative hydrogen-bond networks involved. They include TIM, CS, and chymotrypsin, where H95, H274, and the NH groups of G193 and S195 were proposed to form low-barrier hydrogen bonds with the intermediates. Thus, it is possible that the energetic stabilization might come from the cooperative hydrogen bonding rather than the formation of low-barrier hydrogen bonds per se.

Received: February 24, 1998 [Z11513IE]
German version: *Angew. Chem.* **1998**, *110*, 3155 – 3160

Keywords: cooperative effects · density functional calculations · enzyme catalysis · hydrogen bonds · protein structures

[1] A. J. Kirby, *Angew. Chem.* **1996**, *108*, 770 – 790; *Angew. Chem. Int. Ed. Engl.* **1996**, *35*, 705 – 724.
[2] J. R. Knowles, *Nature* **1991**, *350*, 121 – 125.
[3] a) W. G. J. Hol, P. T. van Duijnen, H. J. C. Berendsen, *Nature* **1978**, *273*, 443 – 446; b) W. G. J. Hol, *Prog. Biophys. Mol. Biol.* **1984**, *45*, 149 – 195.
[4] a) J. A. Gerlt, P. G. Gassman, *Biochemistry* **1993**, *32*, 11943 – 11952; b) W. W. Cleland, M. M. Kreevoy, *Science* **1994**, *264*, 1887 – 1890; c) P. A. Frey, S. A. Whitt, J. B. Tobin, *Science* **1994**, *264*, 1927 – 1930; d) J. A. Gerlt, M. M. Kreevoy, W. W. Cleland, P. A. Frey, *Chem. Biol.* **1997**, *4*, 259 – 267, and references therein.
[5] a) J. Aqvist, H. Luecke, F. A. Quiocho, A. Warshel, *Proc. Natl. Acad. Sci. USA* **1991**, *88*, 2026 – 2030; b) B. Tidor, M. Karplus, *Biochemistry* **1991**, *30*, 3217 – 3228; c) B. Tidor, *Proteins* **1994**, *19*, 310 – 323.
[6] a) J. P. Guthrie, *Chem. Biol.* **1996**, *3*, 163 – 170, and references therein.; b) C. L. Perrin, J. B. Nielson, *Annu. Rev. Phys. Chem.* **1997**, *48*, 511—544, and references therein.; c) A. Warshel, A. Papazyan, P. Kollman, *Science* **1995**, *269*, 102 – 106.
[7] a) R. R. Copley, G. J. Barton, *J. Mol. Biol.* **1994**, *242*, 321 – 329; b) P. Chakrabarti, *J. Mol. Biol.* **1993**, *234*, 463 – 482.
[8] M. M. Benning, K. L. Taylor, R. Q. Liu, G. Yang, H. Xiang, G. Wesenberg, D. Dunaway-Mariano, H. M. Holden, *Biochemistry* **1996**, *35*, 8103 – 8109.
[9] K. Brady, A. Wei, D. Ringe, R. H. Abeles, *Biochemistry* **1990**, *29*, 7600 – 7607.
[10] H. Luecke, F. A. Quiocho, *Nature* **1990**, *347*, 402 – 406.
[11] F. A. Quiocho, J. S. Sack, W. K. Vyas, *Nature* **1987**, *329*, 561 – 564.
[12] a) G. A. Jeffrey, W. Saenger, *Hydrogen bonding in biological structures*, Springer, Berlin, **1991**; b) H. Guo, M. Karplus, *J. Phys. Chem.* **1994**, *98*, 7104—7105, and references therein.; c) H. Guo, M. Karplus, *J. Phys. Chem.* **1992**, *96*, 7273 – 7287; d) B. W. Gung, Z. Zhu,

  1433-7851/98/3721-2989 $ 17.50+.50/0

Tetrahedron Lett. **1996**, *37*, 2189 – 2192; e) B. W. Gung, Z. Zhu, B. Everingham, *J. Org. Chem*. **1997**, *62*, 3436 – 3437; f) J. E. Del Bene, *J. Chem. Phys.* **1980**, *73*, 3423 – 3424.
[13] a) E. N. Baker, R. E. Hubbard, *Prog. Biophys. Mol. Biol*. **1984**, *44*, 97 – 179; b) D. Stickle, L. G. Presta, K. A. Dill, G. D. Rose, *J. Mol. Biol*. **1992**, *226*, 1143 – 1159.
[14] T. Head-Gordon, M. Head-Gordon, M. J. Frisch, C. Brooks III, J. A. Pople, *J. Am. Chem. Soc*. **1991**, *113*, 5989 – 5997.
[15] J. E. H. Koehler, W. Saenger, B. Lesyng, *J. Comput. Chem*. **1987**, *8*, 1090 – 1098.
[16] J. W. Andzelm, M. E. Casida, A. Koester, E. Proynov, A. St-Amant, D. R. Salahub, H. Duarte, N. Godbout, J. Guan, C. Jamorski, M. Leboeuf, V. Malkin, O. Malkina, F. Sim, A. Vela, *deMon Software*, University of Montreal, **1995**.
[17] W. Bode, E. Papamokos, D. Musil, U. Seemuller, H. Fritz, *EMBO J.* **1986**, *5*, 813 – 818.
[18] J. J. He, F. A. Quiocho, *Protein Sci*. **1993**, *2*, 1643 – 1647.
[19] R. C. Davenport, P. A. Bash, B. A. Seaton, M. Karplus, M. G. A. Petsko, D. Ringe, *Biochemistry* **1991**, *30*, 5821 – 5826.

New Protein Mimetics: The Zinc Finger Motif as a Locked-In Tertiary Fold

Gabriele Tuchscherer,* Christian Lehmann, and Marc Mathieu

Dedicated to Professor Murray Goodman on the occasion of his 70th birthday

De novo protein design aims to mimic some of the structural and functional properties of native proteins.[1–6] One of the most intriguing hurdles in this rapidly growing field is the complexity of the folding mechanism, that is, the pathway by which a linear polypeptide chain adopts its unique three-dimensional structure. To bypass this well-known protein-folding problem,[7–9] the concept of template assembled synthetic proteins (TASP) was introduced, in which topological template molecules direct the folding of covalently attached peptide blocks into a predetermined packing arrangement with a branched-chain architecture.[3, 10–12]

Recent progress in the synthetic methodology for assembling peptides allows us now to access the full potential of the TASP approach. For example, by conceptually separating the structural and functional domains of native proteins, we have recently proposed the use of topological templates as structure-supporting scaffolds for the assembly of receptor binding loops.[13] Here we extend the TASP concept of protein design to the construction of proteinlike packing topologies with multiply branched, oligocyclic chain architectures ("locked-in folds"). These synthetic macromolecules exhibit unique physicochemical and folding properties and serve as versatile scaffolds in protein design and mimicry.

[*] Dr. G. Tuchscherer, Dr. C. Lehmann, Dr. M. Mathieu
Institute of Organic Chemistry, University of Lausanne
BCH-Dorigny, CH-1015 Lausanne (Switzerland)
Fax: (+41) 21-692-3955
E-mail: gabriele.tuchscherer@ico.unil.ch

[**] This work was supported by the Swiss National Science Foundation.

As shown in Figure 1, the envisioned structural motif is based on the principles of a molecular kit, in which building blocks such as α helices, β sheets, and loops are assembled by means of templates or spacer molecules to give covalently cross-linked multiply bridged ("locked-in") tertiary folds. Folding into a predetermined three-dimensional structure is

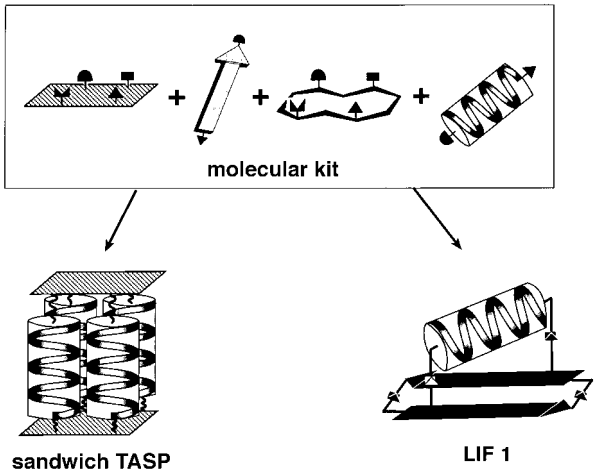

Figure 1. Molecular kit approach in de novo protein design: helices, β sheets, loops, and templates with chemoselectively addressable functional groups (e.g., aldehyde and aminooxy groups; depicted as solid symbols) are the constituents of a molecular kit. A variety of cheomoselective bond-forming methods allows the assembly of these building blocks into locked-in folds (LIF), and the folding problem of linear peptide chains can thus be bypassed.

achieved by the enforced intramolecular association of secondary structure forming peptide blocks to give highly constrained tertiary folds of increased thermodynamic stability. Most importantly, the large number of alternative folding pathways and packing arrangements of linear polypeptide chains is drastically reduced due to the confined conformational space. The proposed concept relies strongly on new methodologies in synthetic peptide chemistry such as chemoselective ligation procedures[14–17] and orthogonal protecting group techniques,[12] which allow the specific assembly of unprotected peptide segments as building blocks according to a molecular kit approach.

Our first aim was to mimic some structural and functional features of a zinc finger motif (finger 1 of Zif268) by a locked-in fold with an overall topology similar to that of the native molecule. Zinc finger proteins contain one of the most interesting structural motifs for the separation of structural and functional domains[13] and for the modulation of DNA-binding specificities.[18, 19] The consensus sequence Xaa_2-Cys-Xaa_{2-4}-Cys-Xaa_{12}-His-Xaa_{2-4}-His-Xaa_4 (Xaa represents variable amino acids)[20, 21] folds in the presence of Zn^{II} ions into a $\beta\beta\alpha$ folded unit, which binds through its helical face to three base pairs of the DNA. Multimeric zinc finger proteins consisting of several zinc finger (Zif) modules play a key role in controlling gene expression.[18, 19]

On applying the general concept of locked-in folds, the $\beta\beta\alpha$ framework of the Zif motif immediately suggests the use of a strategy based on the principles of a molecular kit. The constituent elements are a cyclic β-sheet template that mimics

  1433-7851/98/3721-2990 $ 17.50+.50/0